Network models of photonic Floquet topological insulators

Michael Pasek* and Y. D. Chong†

School of Physical and Mathematical Sciences and Centre for Disruptive Photonic Technologies, Nanyang Technological University, Singapore 637371, Singapore

(Received 26 November 2013; revised manuscript received 27 January 2014; published 13 February 2014)

A recently proposed class of photonic topological insulators is shown to map onto Chalker-Coddington-type networks, which were originally formulated to study disordered quantum Hall systems. Such network models are equivalent to the Floquet states of periodically driven lattices. We show that they can exhibit topologically protected edge states even if all bands have zero Chern number, which is a characteristic property of Floquet band structures. These edge states can be counted by an adiabatic pumping invariant based on the winding number of the coefficient of reflection from one edge of the network.

DOI: 10.1103/PhysRevB.89.075113 PACS number(s): 03.65.Vf, 73.43.−f, 78.67.Pt

I. INTRODUCTION

Since the work of Thouless and co-workers [1], physicists have recognized that the exotic physics encountered in quantum Hall systems [2], and more recently topological insulator materials [3–5], is intimately tied to the topological properties of their band structures. Topological band theory has since been extended in several interesting directions beyond its original context. For example, several groups have shown that when cold-atom or condensed-matter lattices are subjected to a time-periodic drive, the resulting Bloch-Floquet states can form topologically nontrivial bands [6–11]. These "Floquet topological insulators" [10,12] exhibit many of the properties expected of topological materials, such as edge states which are immune to disorder-induced backscattering, but they also have some unique and peculiar characteristics of their own; for example, topologically protected edge states can exist even when all the bands have zero Chern number and would thus normally be considered "topologically trivial" [9,13]. Topological band structures have also been identified in photonic systems, including magneto-optic photonic crystals [14–17], cavity QED circuits [18,19], metamaterial photonic crystals [20], and ring resonator lattices [21–23]. Interest in these systems is driven, in part, by the possible device applications of topologically protected photonic modes (e.g., the stabilization of slow-light transmission), and in part by the fundamental interest of combining topological band physics with optical phenomena (e.g., gain and nonlinearity). The literature on topological photonics has intersected in interesting ways with the Floquet topological insulator concept: notably, Fang *et al*. have studied the Floquet band structures formed by lattices of photonic resonators which are driven periodically (e.g., by electro-optic modulators) [24], while Rechtsman *et al*. have experimentally demonstrated a coupled-waveguide array which acts like a Floquet topological insulator, with adiabatic wave-packet evolution along a spatially modulated axis simulating a time-periodic drive [25]. We will focus on ring resonator lattices of the sort studied in Refs. [21–23]. Such photonic topological insulators have the technologically desirable properties of being on chip, realizable at optical frequencies, and not requiring an external drive or magnetic field. As originally proposed by Hafezi *et al*. [21], ring resonators are arranged in a two-dimensional (2D) lattice, and coupled weakly by specially engineered waveguides which produce phase shifts incommensurate with the lattice, analogous to the Landau gauge in the quantum Hall effect. Subsequently, it was shown that a topological band structure could be obtained in a lattice with commensurate couplings [23], analogous to the zero-field quantum Hall effect [26]. The transition into the topologically nontrivial phase occurs by tuning the inter-ring couplings to large values, such that the system must be treated with transfer-matrix rather than tight-binding methods.

In this paper, we point out that these resonator-and-waveguide photonic topological insulators [21–23] can be modeled as networks of the sort developed by Chalker and Coddington in the 1980s to study the Anderson transition in quantum Hall systems [27–30]. The Bloch modes of *periodic* network models can be mapped onto the Bloch-Floquet states of driven lattices [31–33]. As mentioned above, the latter have attracted a great deal of recent attention [6–13], although ideas from the network model literature have not been widely employed for studying them. As we shall see, the network picture allows a topological invariant to be formulated based on adiabatic pumping [34,35], relating the number of topologically protected edge states in the projected band structure to the winding number of a coefficient of reflection from one edge of the network.

In its original context, a Chalker-Coddington (CC) network model [27] describes a 2D electron gas subject to a strong magnetic field and a smooth disorder potential. In this regime, equipotential contours form a directed network, where each link is associated with an Aharonov-Bohm phase and each node is associated with a unitary scattering matrix

$$S = \begin{bmatrix} \sin\theta e^{i\chi} & -\cos\theta e^{i(\varphi-\xi)} \\ \cos\theta e^{i\xi} & \sin\theta e^{i(\varphi-\chi)} \end{bmatrix}, \tag{1}$$

where θ parametrizes the coupling strength between adjacent links. Although the model was originally formulated for studying the effects of disorder, Ho and Chalker [36] subsequently applied the evolution operator analysis to a periodic square-lattice network, and showed that an effective 2D Dirac Hamiltonian emerges at the critical value $\theta = \pi/4$, with chiral

*mpasek@ntu.edu.sg
†yidong@ntu.edu.sg

edge states appearing when $\theta > \pi/4$. This result was later rederived, in the context of photonic topological insulators, in Ref. [23], together with the bulk and projected band structures. One of the aims of the present paper is to clarify the band topology and the nature of the bulk-edge correspondence in these band structures. It turns out that the band structures derived in Ref. [23] are characteristic of "anomalous Floquet insulators" (AFIs) [9,13]: all bands have zero Chern number despite the existence of topologically protected edge states. We shall also see that network models based on the honeycomb lattice have richer phase diagrams, containing both "Chern insulator" (CI) phases [26] (where the bands have nonzero Chern number) and AFI phases. Similar behavior has previously been found in a 2D hexagonal tight-binding model with periodically varying hopping amplitudes [9].

It is interesting to note that in their original context, network models were intended to be effective descriptions of a system with a definite underlying Hamiltonian—a noninteracting electron gas in a magnetic field and disorder potential. However, the situation is reversed for photonic resonator lattices: here, the wave-amplitude description of coupled ring resonators [37,38] is valid for arbitrary coupling parameters, and an effective Hamiltonian (tight-binding) description emerges for weak coupling [21].

II. PHOTONIC NETWORKS AND FLOQUET MAPS

We begin by examining how a photonic lattice maps onto a network, and how the network may be described by a unitary evolution matrix. As described in Refs. [21–23], and depicted in Fig. 1(a), a photonic topological insulator can be constructed from a lattice of ring resonators. Each resonator acts as an optical waveguide, constraining light to propagate along the ring. Each quarter ring serves as a "link" in a photonic network, which is associated with a phase delay whose value depends on the operating frequency. The direction of propagation in each ring acts as a twofold-degenerate degree of freedom, which can be thought of as an analog of the electron spin in a quantum spin Hall insulator [4]. The primary ring in each unit cell is coupled to its neighbors via waveguide loops [21], shown in Fig. 1(a) as a set of smaller rings. If the couplings have negligible internal backscattering, the inter-ring coupling is "spin" conserving. The clockwise and counterclockwise modes then form separate directed networks; the network for clockwise modes is shown in Fig. 1(b). The interlink couplings, corresponding to the nodes of the network, are described by unitary scattering matrices.

Propagation in such a network can be described by an evolution operator [36,39]. Consider a unit cell of a periodic network, such as the one shown in Fig. 1(b). For each cell, at lattice index n, we can define a surface which is penetrated by q input amplitudes $|a_n\rangle \equiv [a_{1n}, \ldots, a_{qn}]$, and the same number of output amplitudes $|b_n\rangle \equiv [b_{1n}, \ldots, b_{qn}]$. The input and output amplitudes are related by $S_{\text{int}}|a_n\rangle = |b_n\rangle$, where S_{int} is a unitary matrix describing scattering from the interior of the designated surface. As the network is periodic, S_{int} is independent of n. We will focus on the special case where the interior consists of equal-length delay lines with phase delay ϕ, as shown in Fig. 1(b). Then, with appropriate definitions of

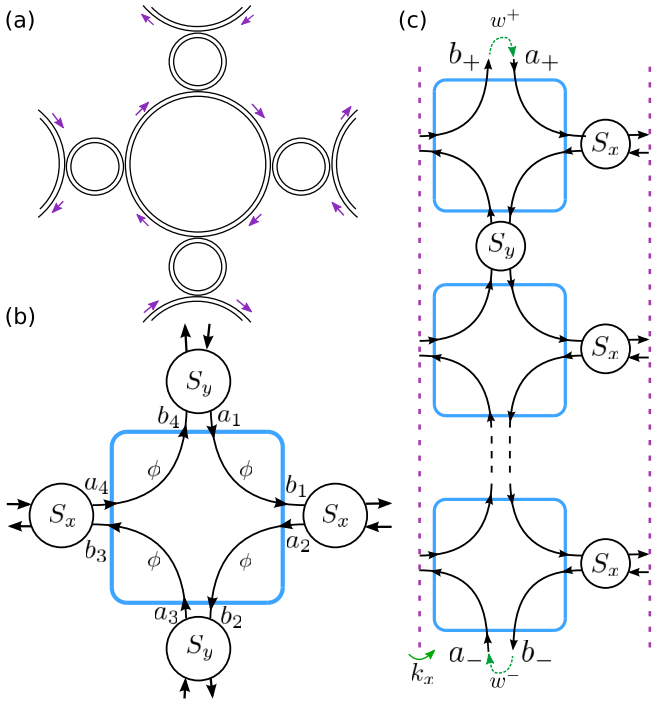

FIG. 1. (Color online) (a) Schematic of a unit cell in a two-dimensional lattice of photonic ring resonators. (b) The equivalent periodic network. Within the unit cell, we define a surface (blue rectangle) which is penetrated by input amplitudes $|a\rangle$ and output amplitudes $|b\rangle$, related by $|b\rangle = e^{i\phi}|a\rangle$. These amplitudes also scatter with those of neighboring cells, with coupling matrices S_x and S_y. (c) A supercell consisting of N_y unit cells joined along the y direction, with twisted boundary conditions along the x direction with twist angle k_x and variable phase delays $w^{\pm}$ along the upper and lower boundaries.

$|a\rangle$ and $|b\rangle$,

$$|a_n\rangle = e^{-i\phi}\,|b_n\rangle. \tag{2}$$

Furthermore, due to the connections between neighboring unit cells, the amplitudes $|b_n\rangle$ leaving the surface of cell n scatter with those from other cells. For Bloch modes $|a_n\rangle = |a_k\rangle e^{ik\cdot r_n}$ and $|b_n\rangle = |b_k\rangle e^{ik\cdot r_n}$, the intercell scattering can be described by

$$S(k)\,|b_k\rangle = |a_k\rangle, \tag{3}$$

where $S(k)$ is unitary and is periodic in k with the periodicity of the Brillouin zone. Combining Eqs. (2) and (3) gives

$$S(k)\,|b_k\rangle = e^{-i\phi}|b_k\rangle. \tag{4}$$

In a photonic structure, the phase delay ϕ is generally proportional to the operating frequency, when working within a limited frequency range. We can regard the eigenvectors $|b_k\rangle$ in Eq. (4) as Bloch wave amplitudes, with $\phi(k)$ playing the role of a band structure, analogous to the band energy of a Bloch electron or the band frequency in a photonic crystal, apart from the fact that it is an angle variable ($\phi \equiv \phi + 2\pi$). Hereafter, we will refer to ϕ as the "quasienergy."

From the above description, we can also see that the Bloch modes of a periodic network are equivalent to the Floquet modes of a periodically driven lattice. Suppose

we have a lattice, of the same spatial dimension as our network, with a Hamiltonian $H_k(t)$ that is periodic in time with period T. Then the Floquet state with state vector $|b_k\rangle$ and Floquet quasienergy $\phi(k)/T$ obeys exactly Eq. (4), provided $S(k)$ is the time-evolution operator over one period. Explicitly,

$$S(k) = \mathcal{T} \exp\left[-i \int_0^T dt\, H_k(t)\right], \tag{5}$$

where $\mathcal{T}$ is the time-ordering operator. Note that an exact expression for $S(k)$ typically cannot be obtained from $H_k(t)$ or vice versa; but it can be computed numerically.

This relationship between network models and Floquet lattices has previously been pointed out [31–33]. One can regard $S(k)$ as a discrete time-evolution operator acting on a particle which is initially localized at one point in the network (say the midpoint of a link); over one time period, the particle moves along the link, tunnels instantaneously across a node, and moves midway along a neighboring link [36]. To our knowledge, however, the consequences of this relationship for the band topology of network models have not been systematically explored.

III. FLOQUET BAND TOPOLOGY OF NETWORK MODELS

Let us consider how the topology of a periodic network's band structure might be characterized. Following the usual topological classification of band insulators [40–42], one might take the matrix logarithm of Eq. (4) to obtain an effective time-independent Hamiltonian, then look for topologically nontrivial bands by computing topological band invariants (e.g., the Chern number for a 2D lattice without time-reversal symmetry [1]). However, doing so for the square-lattice network in the large-θ phase reveals that the Chern number is zero despite the presence of topologically protected "one-way" edge states. As discussed in Ref. [13], such anomalous Floquet insulator behavior can arise in Floquet band structures because the quasienergy ϕ is an angle variable. At the topological transition, each band has simultaneous Dirac band-crossing points with the band "above" and the band "below," modulo 2π; these band-crossing points are respectively associated with $+1$ and -1 Berry flux, so that the band has zero Chern number on both sides of the transition. In a static gapped Hamiltonian system, the number of chiral edge states in a bulk gap can be related to the sum of Chern numbers for all bands below the gap, but this does not apply to Floquet systems since the quasienergy ϕ of a Floquet evolution operator is periodic and not bounded below.

The square-lattice network has a rather simple phase diagram: it is an AFI for values of the inter-ring coupling strength $\theta > \pi/4$, and a conventional insulator otherwise, regardless of all other model parameters (see the projected band structures shown in Fig. 4).

More complicated behaviors can be observed in other network models, such as networks based on a honeycomb lattice. To our knowledge, such networks have not been studied previously, partly because the network model literature was focused on the Anderson transition, and the lattice geometry was not thought to have a significant influence on properties

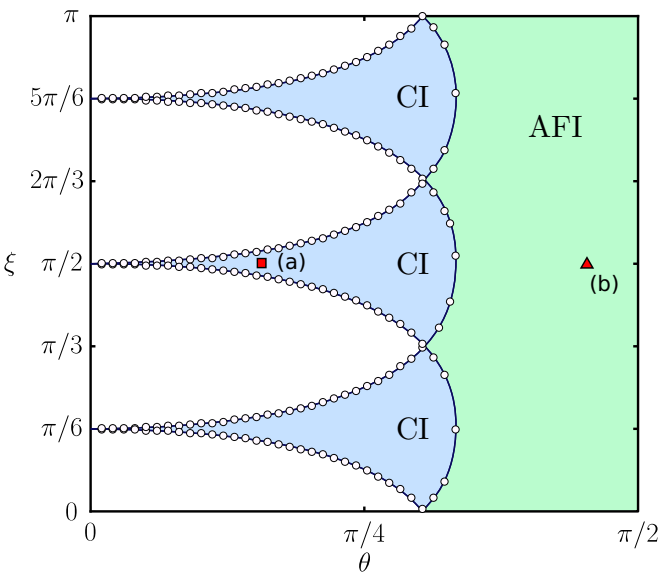

FIG. 2. (Color online) Phase diagram of a honeycomb network. The network is described in Appendix B; here we take the coupling matrix parameters $\varphi = \chi = 0$. The phase boundaries are found by searching numerically for band crossings (dots). The topological nature of each phase is determined by computing the Chern number of each bulk band, as well as counting the number of edge states in the strip geometry. In the Chern insulator phase, bands have nonzero Chern numbers and are separated by band gaps with one-way edge states (as well as band gaps with no edge states). In anomalous Floquet insulator phases, each band has zero Chern number but each band gap has a pair of one-way edge states. The unlabeled phases are conventional insulators. The points labeled (a) and (b) indicate the parameters used for the projected band diagrams in Fig. 3(a) and 3(b), respectively.

such as the critical exponent of the localization length [27]. The honeycomb network, which is described in Appendix B, has phases that depend on the inter-ring coupling θ as well as on the parameters ξ and φ, which describe the phase shifts induced at the nodes [cf. Eqs. (1) and (B22)]. The phase diagram for $\varphi = 0$ is shown in Fig. 2. Unlike in the square lattice, topologically nontrivial phases exist even for low values of θ. In these low-θ Chern insulator phases, the bands have nonzero Chern number, similarly to 2D systems with broken time-reversal symmetry [26], and the projected band structure exhibits topological edge states as shown in Fig. 3(a). At larger values of θ, the system undergoes a transition from a CI phase to an AFI phase, where all bands have zero Chern number and *all* band gaps are traversed by topologically protected edge states [9,13], as shown in Fig. 3(b).

As pointed out by Kitagawa *et al.*, Floquet band structures can be characterized by homotopy-class-based topological invariants [9], such as the "ν_1 invariants"

$$\frac{1}{2\pi} \int_{-\pi}^{\pi} dk_\mu \mathrm{Tr}\left[S(k)^{-1}\, i\partial_{k_\mu} S(k)\right]$$

for $\mu = x, y$ in 2D. In simple terms, these are the winding numbers for the quasienergy bands over their $[0, 2\pi]$ domain, as k_μ is advanced through $[0, 2\pi]$. They are nonzero in the AFI phase, where every band gap is topologically nontrivial

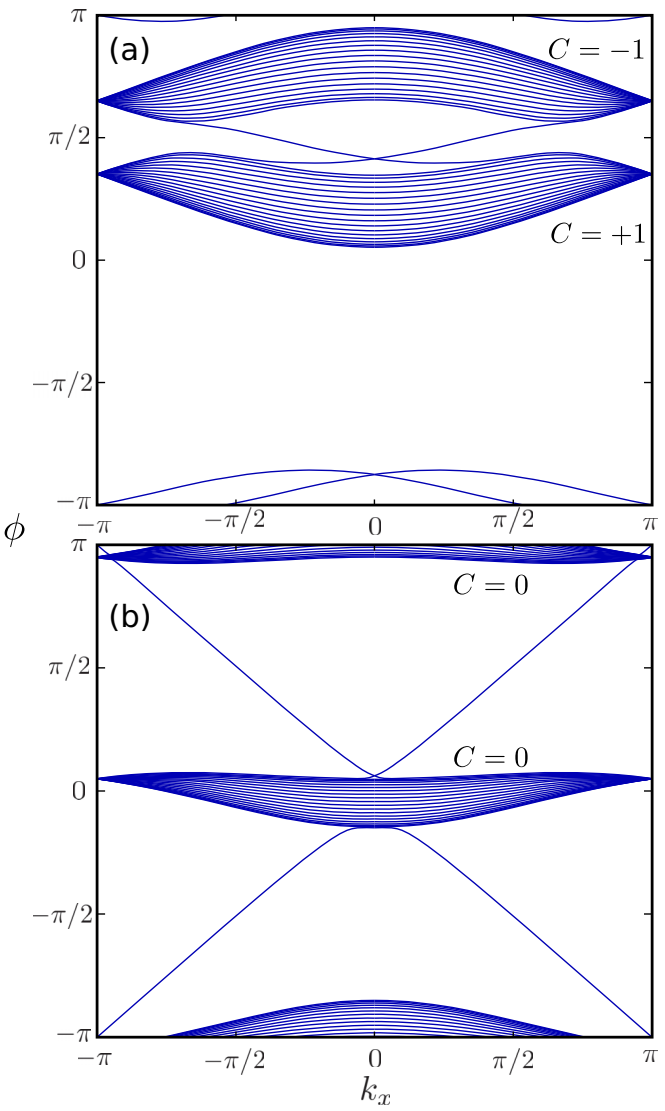

FIG. 3. (Color online) Projected quasienergy band structures for the honeycomb network, in a strip geometry with width $N = 20$ unit cells and zigzag edges. The bands are computed from Eq. (B16); see Fig. 7 for a schematic of the network. The coupling parameters are $\xi = \pi/2$, $\varphi = \chi = 0$, and (a) $\theta = 0.15\pi$ (CI phase; upper figure), (b) $\theta = 0.45\pi$ (AFI phase; lower figure). The Chern number C for each band is indicated. These Chern numbers were computed from the momentum-space line integral of the Berry connection $\mathcal{A}^{nn}(k) = -i\langle nk|\nabla_k|nk\rangle$, where $|nk\rangle$ is the nth Bloch eigenstate [1].

and occupied by edge states; however, the winding numbers are zero in CI phases where at least one of the band gaps is topologically trivial [9]. Subsequently, Rudner *et al.* have shown that the nontrivial topology of both the AFI and CI phases can be characterized by a bulk ν_3 invariant [13]. This invariant involves integrals over k_x and k_y, and over the time variable t. In the context of network models, there is no meaningful definition of the "evolution operator" for intermediate t. In practice, one can define any $S(k,t)$, such that $S(k,T)$ is the evolution operator for the network; the choice is nonunique but will not affect the value of ν_3 thus obtained.

In the following section, we will investigate an alternative topological characterization based on adiabatic pumping. As we shall see, the adiabatic pumping procedure is also capable of distinguishing the AFI and CI phases, and it has the additional advantage of having a natural physical interpretation for network models, which could be useful for understanding the general class of Floquet band structures.

IV. ADIABATIC PUMPING METHOD AND EDGE-STATE INVARIANTS

The adiabatic pumping method of characterizing topological systems was originally introduced by Laughlin [34], and we will adapt an elegant reformulation of the Laughlin argument which was recently given by Meidan *et al.* [35]. Working in the context of static Hamiltonian systems, these authors imagined rolling a 2D lattice into a cylinder, attaching scattering leads to one cylinder edge, and then calculating the eigenvalues of the scattering (reflection) matrix. As one magnetic flux quantum is threaded through the cylinder, the scattering eigenvalues acquire phase shifts which can be related, via standard scattering theory, to the number of resonances crossing the specified energy. For midgap energies, scattering resonances correspond to edge states of the isolated cylinder, and these can be counted by the winding numbers of the scattering matrix's eigenvalues [35].

A related procedure can be carried out for a network model. Let us consider a two-dimensional network, which is infinite in (say) the x direction, and finite in the y direction with N_y periods. For convenience, we normalize the lattice spacings so the quasimomentum k_x becomes an angle variable. The system can be regarded as a supercell of N_y unit cells, featuring twisted boundary conditions along the x boundaries with twist angle k_x: translating one unit in the $+x$ direction is equivalent to multiplying the wave amplitude by $\exp(ik_x)$. Following the discussion in Sec. II, we can designate a scattering surface for this supercell, consisting of the union of the scattering surfaces for the individual unit cells. This is shown in Fig. 1(c) for the simple square-lattice network. The inputs entering this supercell surface are $|a\rangle = [|a_1\rangle, \ldots, |a_{N_y}\rangle]$, and the output amplitudes are $|b\rangle = [|b_1\rangle, \ldots, |b_{N_y}\rangle]$. The scattering from the interior of the surface gives $|a\rangle = e^{-i\phi}|b\rangle$. As for the scattering from the exterior of the surface back into the interior, that depends on the intercell connections (which are assumed constant), and on k_x (due to scattering across the x boundaries). There is one more set of constraints which must also be specified: the relations between the input and output amplitudes penetrating the scattering surface along the y boundaries of the supercell. As depicted in Fig. 1(c), we denote these "edge amplitudes" by $|a_\pm\rangle$ and $|b_\pm\rangle$, with the $\pm$ subscripts indicating the upper and lower edges. Let the number of edge amplitudes on each edge be $n_\perp$. In general, we have

$$S_\perp \begin{bmatrix} |b_+\rangle \\ |b_-\rangle \end{bmatrix} = \begin{bmatrix} |a_+\rangle \\ |a_-\rangle \end{bmatrix} \tag{6}$$

for some $2n_\perp \times 2n_\perp$ unitary matrix $S_\perp$. From this, we can construct an exterior scattering matrix for the supercell, $S_{\rm sc}$, such that

$$S_{\rm sc}(k_x, S_\perp)|b\rangle = e^{-i\phi}|b\rangle. \tag{7}$$

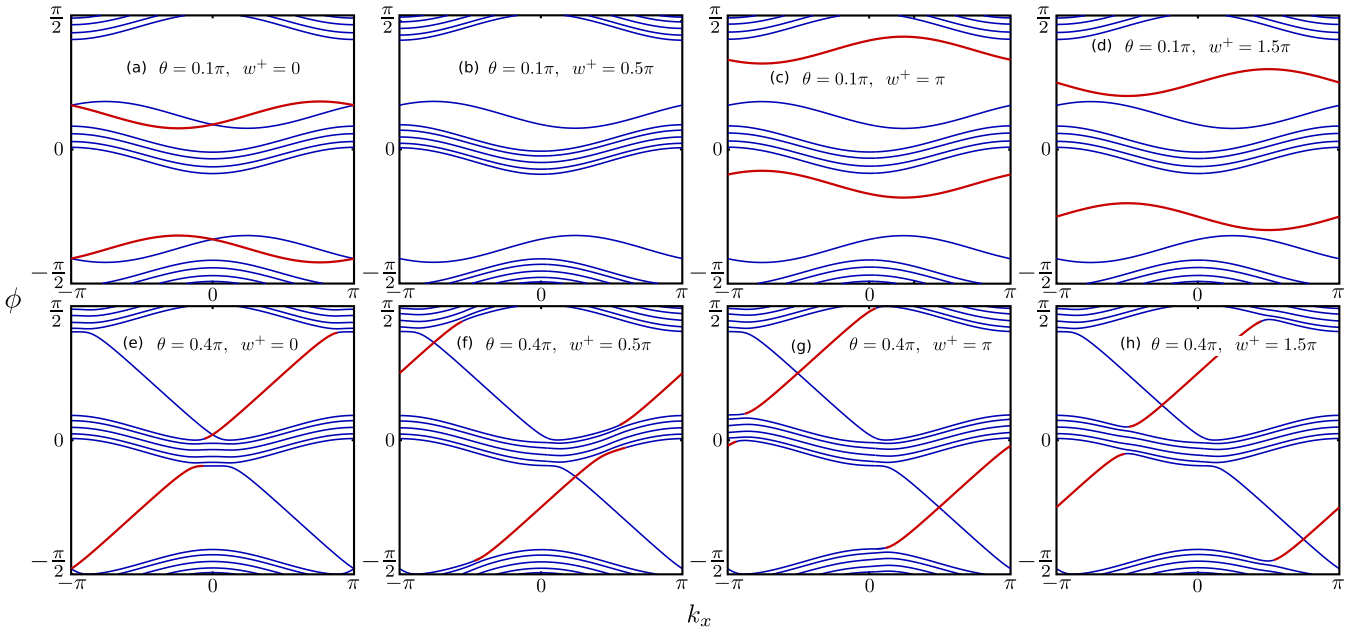

FIG. 4. (Color online) Projected band structures for the periodic square-lattice network of Fig. 1(c), with $N_y = 6$ periods in the y direction. (a)–(d) show topologically trivial band structures ($\theta = 0.1\pi$, where θ is the inter-ring coupling strength [23]), and (e)–(h) show topologically nontrivial band structures ($\theta = 0.4\pi$). Varying w^+, the angle variable controlling the upper edge, affects the edge states on the upper edge (highlighted in red). The lower edge angle is fixed at $w^- = 0$, and the other coupling matrix parameters [23] are $\varphi = \chi = 0$, $\xi = \pi/2$.

We are free to specify $S_\perp$, and it is useful to consider a case where the upper and lower boundaries are "disconnected." Specifically,

$$S_\perp(w^+, w^-) = \begin{bmatrix} e^{iw^+} I & 0 \\ 0 & e^{iw^-} I \end{bmatrix}. \tag{8}$$

The values of $\phi(k_x)$ obtained from Eqs. (7) and (8) form a projected quasienergy band structure for the semi-infinite lattice of width N_y, with the set of $2n_\perp$ edge angles $\{w^\pm\}$ acting as tunable edge conditions.

The edge angles $w^\pm$ can be used to define topological edge invariants. Suppose we keep w^- fixed and consider only variations in w^+. For any $\phi, k_x \in [0, 2\pi]$, there must be exactly $n_\perp$ values of $w^+ \in [0, 2\pi]$ consistent with Eqs. (7) and (8); in physical terms, by specifying ϕ and k_x (as well as fixing w^- and other network parameters entering into $S_{\rm sc}$), we have defined an $n_\perp$-channel scattering problem, and the input amplitudes $|a_+\rangle$ and output amplitudes $|b_+\rangle$ for the scatterer must be related by some unitary reflection matrix whose eigenvalues are e^{iw^+}. Let us fix a value for the quasienergy ϕ which lies in a bulk band gap, and consider the $n_\perp$-valued function $w^+(k_x)$, which must come back to itself (modulo 2π) as k_x is advanced over $[0, 2\pi]$. Each value of w^+ corresponds to a separate projected band structure, but within each gap only the dispersion curves for edge states localized to the upper edge can vary, since w^+ cannot affect the lower edge. As a result, the winding number of $w^+(k_x)$ counts the net (forward minus backward) number of upper edge states in the specified band gap. By evaluating the w^+ edge invariants in each band gap, we can determine the Chern number of each band, which is the difference between the invariants for the band gaps above and below the band [13].

To illustrate the above discussion, consider the previously discussed square-lattice network, for which $n_\perp = 1$ [i.e., $w^+(k_x)$ is single-valued]. Projected band structures for this network are shown in Fig. 4; for details of the calculation, see Appendix A. In the conventional insulator phase, corresponding to Figs. 4(a)–4(d), $w^+(k_x)$ has zero winding number in each gap, as shown in Fig. 5(a). Note, however, that Fig. 5(a) also shows that there are certain values of w^+ for which upper edge states *do* exist. In the projected band structure, these take the form of isolated bands of *two-way* edge states which are "pumped" downwards across each gap during each cycle of w^+.

In the AFI phase, $w^+(k_x)$ has winding number $+1$ in each gap, as shown in Fig. 5(b). The projected band structures, shown in Figs. 4(e)–4(h), exhibit one-way edge states spanning each gap. Each band of edge states "winds" across the Brillouin zone during one cycle of w^+, with the overall effect of pumping one band down across each gap during one cycle of w^+, as in the conventional insulator phase. Each gap also has a band of edge states that is invariant in w^+, corresponding to states localized on the lower edge. We expect this to be the generic effect of adiabatic pumping on quasienergy band structures. Because w^+ is a well-defined function of k_x, winding w^+ by 2π has the effect of transporting a band of edge states across each gap. This transport occurs even for conventional (topologically trivial) band gaps, in the form of a band of two-way edge states. The band structure as a whole returns to itself over one such cycle, which is possible since the quasienergy is an angle variable.

In the honeycomb network, the conventional insulator and AFI phases behave in the same way as for the square-lattice network. In the CI phase, each cycle of w^+ transports a band of two-way edge states down across the topologically trivial

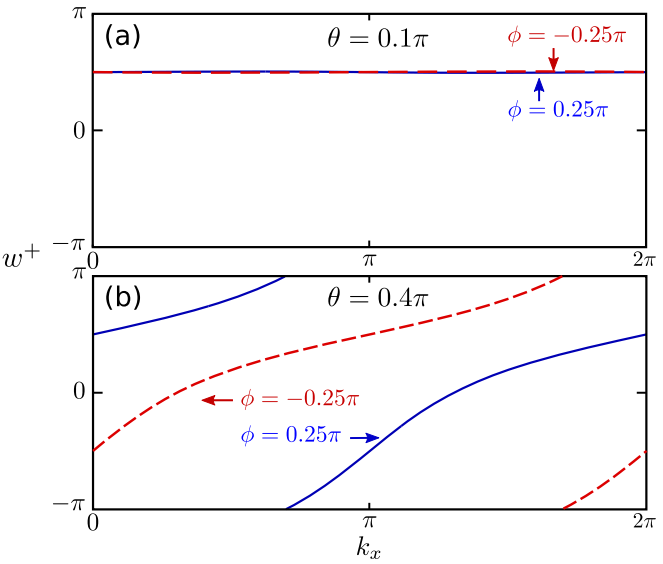

FIG. 5. (Color online) Plots of the edge angle w^+ versus k_x, in the square-lattice network with width $N_y = 6$. (a) In the conventional insulator phase ($\theta = 0.1\pi$), the winding numbers are zero; (b) in the AFI phase ($\theta = 0.4\pi$), the winding numbers are $+1$. In both cases, plots are given for $\phi = \pi/4$ and $\phi = -\pi/4$, which lie in two different band gaps (see Fig. 4). In all cases, $w^- = 0$ and all the other parameters are the same as in Fig. 4.

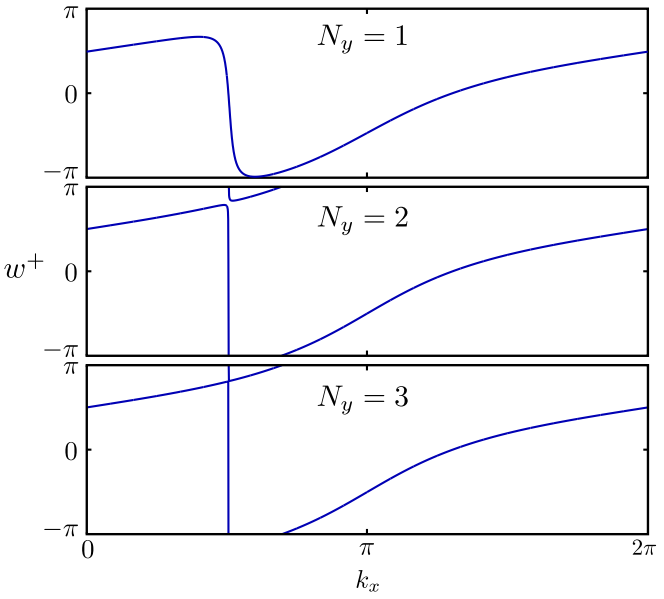

FIG. 6. (Color online) Plots of w^+ versus k_x for small values of N_y, showing the emergence of a nonzero winding number. For all three plots, we use $\phi = 0.25\pi$ and $\theta = 0.4\pi$, corresponding to a midgap quasienergy in the AFI phase. All other parameters are as in Fig. 4. For $N_y > 1$, an anticrossing develops near $k_x \sim \pi/2$, coinciding with the dispersion curve for the lower edge states in the projected band diagram. The width of this anticrossing goes rapidly to zero with N_y, and the rest of the curve acquires a nonzero winding number.

gaps [where $w^+(k_x)$ has zero winding number], while simultaneously winding the one-way edge states in the topological gaps [where $w^+(k_x)$ has winding number ± 1]. For example, for the band with Chern number $+1$ shown in Fig. 3(a), w^+ has winding number $+1$ in the band gap above and 0 in the band gap below.

The relation of the winding number of $w^+(k_x)$ to the edge states relies on the assumption that the upper edge angles have no effect on the lower edge states. Hence, ϕ must be chosen within a band gap, and the width N_y must be sufficiently large (compared to the edge state penetration depth). This is demonstrated in Fig. 6, where we plot $w^+(k_x)$ using $N_y = 1,2,3$ for the square-lattice network in the AFI phase. For $N_y = 1$, we observe that $w^+(k_x)$ has zero winding number. As N_y is increased, the curve develops an anticrossing, occurring at a value of k_x coinciding with the quasimomentum of an edge state localized to the lower edge (for the specified value of ϕ). For sufficiently large N_y, the lower edge state is independent of w^+, so the anticrossing narrows into a numerically undetectable vertical line. Because the anticrossing is associated with a -1 winding number, the remainder of the $w^+(k_x)$ curve acquires $+1$ winding.

For recent related works on the measurement of topological properties in 2D photonic lattices, see Refs. [43–45].

V. DISCUSSION

In this paper, we have discussed the relationships between photonic resonator lattices, Chalker-Coddington network models, and Floquet topological insulators. Within the emerging field of topological photonics, these analogies may provide insights for realizing additional topological phases. For example, some years ago Chalker and Dohmen [46] studied a hypothetical three-dimensional network consisting of weakly coupled 2D stacked layers of CC networks (a configuration reminiscent of a 3D weak topological insulator [4]). Photonic lattice analogs of such 3D networks may be realizable, possibly at microwave frequencies for ease of fabrication. Furthermore, as discussed in the Introduction, a photonic Floquet topological insulator has recently been realized [25], in which the 2D bands were shown to possess nonzero Chern numbers. It would be interesting to analyze this or a similar system using the scattering formalism of a network model, with the aim of realizing an AFI phase where topologically protected edge states are present despite all bands having zero Chern number. (A photonic AFI-like phase has previously been realized in 1D [47]).

We have restricted our attentions to *directed* network models. In the photonic context, this means considering the flow of light in a single direction within the waveguides, and assuming no backscattering into time-reversed modes. Apart from this restriction, there are no further symmetry requirements on the coupling matrices. The two possible directions of propagation through the network are analogous to two decoupled spin sectors in a 2D quantum spin Hall insulator. However, in the electronic case a topological phase can exist even in the presence of spin mixing: the $\mathbb{Z}_2$ topological insulator. This relies on the fact that edge states cannot be backscattered by time-reversal-symmetric perturbations due to the particular nature of *fermionic* time-reversal-symmetric S matrices [4]. Indeed, the CC network model concept has been generalized to study quantum spin Hall insulators by

imposing fermionic time-reversal symmetries on the links and nodes [48–50]. However, *bosonic* edge states are not protected from backscattering by time-reversal-symmetric perturbations, so topologically nontrivial behavior can occur only if mixing into time-reversed modes is negligible. This is an important limitation of photonic topological insulators, but not necessarily a fatal one, since such mixing processes can often be engineered away.

We have also, in this paper, considered translationally periodic systems. It would be interesting to return to the original motivation for introducing network models, which was to study disorder-induced Anderson transitions in a 2D electron gas [27]. In the photonic context, Anderson *localization* of light has been observed in 1D and 2D [51,52]. However, there is no Anderson *transition* in such systems, since they map onto time-reversal-symmetric electron gases for which localization is marginal in 2D [53]. By contrast, an Anderson transition does exist in 2D disordered quantum Hall systems, tied to the phenomenon of classical percolation [27]. Random photonic networks might thus manifest a photonic localization-delocalization transition, which has not yet been observed.

ACKNOWLEDGMENTS

We thank M. Rechtsman, A. Szameit, M. Hafezi, and G. Q. Liang for helpful comments. This research was supported by the Singapore National Research Foundation under Grant No. NRFF2012-02.

APPENDIX A: BAND STRUCTURE OF A SQUARE-LATTICE NETWORK

Figure 1(b) shows a unit cell of the square-lattice network, which consists of two nodes with coupling relations

$$S_x \begin{bmatrix} b_{1,n} \\ b_{3,n+x} \end{bmatrix} = \begin{bmatrix} a_{4,n+x} \\ a_{2,n} \end{bmatrix}, \tag{A1}$$

$$S_y \begin{bmatrix} b_{4,n} \\ b_{2,n+y} \end{bmatrix} = \begin{bmatrix} a_{3,n+y} \\ a_{1,n} \end{bmatrix}, \tag{A2}$$

where

$$S_\mu = \begin{bmatrix} r_\mu & t'_\mu \\ t_\mu & r'_\mu \end{bmatrix}. \tag{A3}$$

Using the relations between wave amplitudes $a_{i,n}$ and $b_{i,n}$ coming from link phases, we can write Eq. (A2) as

$$S_y \begin{bmatrix} a_{4,n} \\ a_{2,n+y} \end{bmatrix} = \begin{bmatrix} b_{3,n+y} \\ b_{1,n} \end{bmatrix} e^{-2i\phi}. \tag{A4}$$

From the translational invariance of the network strip in the x direction, the wave amplitudes in Eq. (A1) can be written in the Bloch form to obtain

$$S_x \begin{bmatrix} b_{1,n} \\ b_{3,n} e^{ik_x} \end{bmatrix} = \begin{bmatrix} a_{4,n} e^{ik_x} \\ a_{2,n} \end{bmatrix}. \tag{A5}$$

By reordering the terms in (A4) and (A5), one obtains

$$S'_x(k_x) \begin{bmatrix} b_{3,n} \\ b_{1,n} \end{bmatrix} = \begin{bmatrix} a_{2,n} \\ a_{4,n} \end{bmatrix}, \tag{A6}$$

$$S'_y \begin{bmatrix} a_{4,n} \\ a_{2,n+y} \end{bmatrix} = \begin{bmatrix} b_{1,n} \\ b_{3,n+y} \end{bmatrix} e^{-2i\phi}. \tag{A7}$$

In order to obtain the band structure of the square-lattice network in the strip geometry, we need to construct a scattering matrix for the supercell, $S_{\rm sc}$, defined in Fig. 1(c). This obeys

$$S_{\rm sc}(k_x, w^+, w^-)|b\rangle = e^{-i\phi T}|b\rangle, \tag{A8}$$

where $|b\rangle$ is a wave-amplitude vector, and the angles w^+ and w^- set the boundary conditions at the strip edges such that (cf. Fig. 1)

$$e^{iw^-} b_{2,1} = a_{3,1}, \tag{A9}$$

$$e^{iw^+} b_{4,N_y} = a_{1,N_y}, \tag{A10}$$

or, equivalently,

$$e^{iw^-} a_{2,1} = b_{3,1} e^{-2i\phi}, \tag{A11}$$

$$e^{iw^+} a_{4,N_y} = b_{1,N_y} e^{-2i\phi}. \tag{A12}$$

Finally, using Eqs. (A6), (A7), (A11), and (A12) one can construct the $2N_y \times 2N_y$ matrices M_A and M_B such that

$$M_A(w^+, w^-) = \begin{bmatrix} e^{iw^-} & & & & \\ & S'_y & & & \\ & & \ddots & & \\ & & & S'_y & \\ & & & & e^{iw^+} \end{bmatrix}, \tag{A13}$$

$$M_B(k_x) = \begin{bmatrix} S'_x & & \\ & \ddots & \\ & & S'_x \end{bmatrix}, \tag{A14}$$

to obtain

$$M_A(w^+, w^-) M_B(k_x)|b'\rangle = e^{-2i\phi}|b'\rangle, \tag{A15}$$

where $|b'\rangle = [b_{3,1}, b_{1,1}, \ldots, b_{3,N_y}, b_{1,N_y}]$, which is similar to Eq. (A8) with $T = 2$.

APPENDIX B: BAND STRUCTURE AND PHASE DIAGRAM OF A HONEYCOMB NETWORK

The honeycomb network unit cell is represented in Fig. 7, with the corresponding wave amplitudes. We define the scattering relations at the nodes of the network such that the first (second) reflection block of the S matrix describes the hopping in the $+\delta_i$ $(-\delta_i)$ direction, where $i = 1,2,3$.

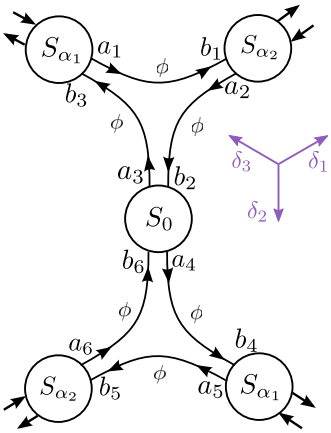

FIG. 7. (Color online) Schematic of a unit cell in a two-dimensional honeycomb periodic network.

This gives

$$S_{\alpha_2}\begin{bmatrix} b_{1,n} \\ b_{5,n+\alpha_2} \end{bmatrix} = \begin{bmatrix} a_{6,n+\alpha_2} \\ a_{2,n} \end{bmatrix}, \tag{B1}$$

$$S_{\alpha_1}\begin{bmatrix} b_{3,n} \\ b_{4,n+\alpha_1} \end{bmatrix} = \begin{bmatrix} a_{5,n+\alpha_1} \\ a_{1,n} \end{bmatrix}, \tag{B2}$$

$$S_0\begin{bmatrix} b_{2,n} \\ b_{6,n} \end{bmatrix} = \begin{bmatrix} a_{4,n} \\ a_{3,n} \end{bmatrix}. \tag{B3}$$

Using the phase relations on network links, we can rewrite Eqs. (B1)–(B3) as

$$S_{\alpha_2}\begin{bmatrix} b_{1,n} \\ b_{5,n+\alpha_2} \end{bmatrix} = \begin{bmatrix} a_{6,n+\alpha_2} \\ a_{2,n} \end{bmatrix}, \tag{B4}$$

$$S_{\alpha_1}\begin{bmatrix} a_{3,n} \\ a_{4,n+\alpha_1} \end{bmatrix} = \begin{bmatrix} b_{5,n+\alpha_1} \\ b_{1,n} \end{bmatrix} e^{-2i\phi}, \tag{B5}$$

$$S_0\begin{bmatrix} a_{2,n} \\ a_{6,n} \end{bmatrix} = \begin{bmatrix} a_{4,n} \\ a_{3,n} \end{bmatrix} e^{-i\phi}. \tag{B6}$$

We can now use Bloch's theorem, taking the honeycomb network to be translationally invariant in the $\boldsymbol{\alpha_2}$ direction (which yields zigzag edges). Equations (B5) and (B4) become

$$S'_{\alpha_1}\begin{bmatrix} a_{3,n} \\ a_{4,n+\alpha_1} \end{bmatrix} = \begin{bmatrix} b_{1,n} \\ b_{5,n+\alpha_1} \end{bmatrix} e^{-2i\phi} \tag{B7}$$

$$S'_{\alpha_2}(k)\begin{bmatrix} b_{5,n} \\ b_{1,n} \end{bmatrix} = \begin{bmatrix} a_{2,n} \\ a_{6,n} \end{bmatrix}. \tag{B8}$$

We have the edge angle relations as

$$e^{iw^-} b_{4,1} = a_{5,1}, \tag{B9}$$

$$e^{iw^+} b_{3,N_{\alpha_1}} = a_{1,N_{\alpha_1}}, \tag{B10}$$

or, equivalently,

$$e^{iw^-} a_{4,1} = b_{5,1} e^{-2i\phi}, \tag{B11}$$

$$e^{iw^+} a_{3,N_{\alpha_1}} = b_{1,N_{\alpha_1}} e^{-2i\phi}. \tag{B12}$$

One can thus construct the following matrices:

$$M_A(w^+,w^-) = \begin{bmatrix} e^{iw^-} & & & & \\ & S'_{\alpha_1} & & & \\ & & \ddots & & \\ & & & S'_{\alpha_1} & \\ & & & & e^{iw^+} \end{bmatrix}, \tag{B13}$$

$$M_B = \begin{bmatrix} S_0 & & \\ & \ddots & \\ & & S_0 \end{bmatrix}, \tag{B14}$$

$$M_C(k) = \begin{bmatrix} S'_{\alpha_2} & & \\ & \ddots & \\ & & S'_{\alpha_2} \end{bmatrix}, \tag{B15}$$

such that

$$M_A(w^+,w^-) M_B M_C(k) |b'\rangle = e^{-3i\phi} |b'\rangle, \tag{B16}$$

where $|b'\rangle = [b_{5,1}, b_{1,1}, \ldots, b_{5,N_y}, b_{1,N_y}]$. From these relations, the projected band structure can be computed numerically for each value of w^+ and w^-. The resulting projected band structure for the strip geometry with zigzag edges and $w^+ = w^- = 0$ is shown in Fig. 3. We have also verified that similar edge states are present for armchair edges.

Returning to Eqs. (B1)–(B3), we can derive the bulk band structure, and hence the phase diagram. Setting $S_{\alpha_1} = S_{\alpha_2} = S_0$ for simplicity, we can use the phase-delay relations between amplitudes on the honeycomb network to eliminate a_1, a_3, a_4, a_5 and b_2, b_6. Then Eqs. (B1)–(B3) reduce to

$$r b_1 + t' b_5 e^{i\boldsymbol{k}\cdot\boldsymbol{\alpha_2}} = a_6 e^{i\boldsymbol{k}\cdot\boldsymbol{\alpha_2}}, \tag{B17a}$$

$$t b_1 + r' b_5 e^{i\boldsymbol{k}\cdot\boldsymbol{\alpha_2}} = a_2, \tag{B17b}$$

$$r b_3 + t' b_4 e^{i\boldsymbol{k}\cdot\boldsymbol{\alpha_1}} = b_5 e^{-i\phi} e^{i\boldsymbol{k}\cdot\boldsymbol{\alpha_1}}, \tag{B17c}$$

$$t b_3 + r' b_4 e^{i\boldsymbol{k}\cdot\boldsymbol{\alpha_1}} = b_1 e^{-i\phi}, \tag{B17d}$$

$$r a_2 e^{i\phi} + t' a_6 e^{i\phi} = b_4 e^{-i\phi}, \tag{B17e}$$

$$t a_2 e^{i\phi} + r' a_6 e^{i\phi} = b_3 e^{-i\phi}. \tag{B17f}$$

Here we have used Bloch's theorem, e.g., $b_{5,n+\alpha_2} = b_5 e^{i\boldsymbol{k}\cdot\boldsymbol{\alpha_2}}$ (discarding the index n). With Eqs. (B17e) and (B17f),we can

eliminate b_3 and b_4:

$$rb_1 + t'b_5 e^{i\boldsymbol{k}\cdot\boldsymbol{\alpha}_2} = a_6 e^{i\boldsymbol{k}\cdot\boldsymbol{\alpha}_2}, \tag{B18a}$$

$$tb_1 + r'b_5 e^{i\boldsymbol{k}\cdot\boldsymbol{\alpha}_2} = a_2, \tag{B18b}$$

$$r[ta_2 e^{i2\phi} + r'a_6 e^{i2\phi}] + t'e^{i\boldsymbol{k}\cdot\boldsymbol{\alpha}_1}[ra_2 e^{i2\phi} + t'a_6 e^{i2\phi}] = b_5 e^{-i\phi} e^{i\boldsymbol{k}\cdot\boldsymbol{\alpha}_1}, \tag{B18c}$$

$$t[ta_2 e^{i2\phi} + r'a_6 e^{i2\phi}] + r'e^{i\boldsymbol{k}\cdot\boldsymbol{\alpha}_1}[ra_2 e^{i2\phi} + t'a_6 e^{i2\phi}] = b_1 e^{-i\phi}. \tag{B18d}$$

Finally, using Eqs. (B18a) and (B18b), we eliminate a_2 and a_6 to obtain

$$\begin{aligned} &b_1[rt^2 e^{i2\phi} + r^2 r' e^{-i\boldsymbol{k}\cdot\boldsymbol{\alpha}_2} e^{i2\phi} + rtt' e^{i\boldsymbol{k}\cdot\boldsymbol{\alpha}_1} e^{i2\phi} + rt'^2 e^{i\boldsymbol{k}\cdot(\boldsymbol{a}_1-\boldsymbol{\alpha}_2)} e^{i2\phi}] \\ &\quad = b_5[e^{-i\phi} e^{i\boldsymbol{k}\cdot\boldsymbol{\alpha}_1} - rr't e^{i\boldsymbol{k}\cdot\boldsymbol{\alpha}_2} e^{i2\phi} - rr't'e^{i2\phi} - rr't'e^{i\boldsymbol{k}\cdot(\boldsymbol{\alpha}_1+\boldsymbol{\alpha}_2)} e^{i2\phi} - t'^3 e^{i\boldsymbol{k}\cdot\boldsymbol{\alpha}_1} e^{i2\phi}] \end{aligned} \tag{B19}$$

and

$$\begin{aligned} &b_5[r't^2 e^{i\boldsymbol{k}\cdot\boldsymbol{\alpha}_2} e^{i2\phi} + r'tt' e^{i2\phi} + rr'^2 e^{i\boldsymbol{k}\cdot(\boldsymbol{\alpha}_1+\boldsymbol{\alpha}_2)} e^{i2\phi} + r't'^2 e^{i\boldsymbol{k}\cdot\boldsymbol{\alpha}_1} e^{i2\phi}] \\ &\quad = b_1[e^{-i\phi} - t^3 e^{i2\phi} - rr't e^{-i\boldsymbol{k}\cdot\boldsymbol{\alpha}_2} e^{i2\phi} - rr't e^{i\boldsymbol{k}\cdot\boldsymbol{\alpha}_1} e^{i2\phi} - rr't' e^{i\boldsymbol{k}\cdot(\boldsymbol{\alpha}_1-\boldsymbol{\alpha}_2)} e^{i2\phi}]. \end{aligned} \tag{B20}$$

After simplification, this yields

$$e^{i6\phi}(rr' - tt')^3 + e^{i3\phi}\{t^3 + t'^3 + rr'[te^{i\boldsymbol{k}\cdot\boldsymbol{\alpha}_1} + t'e^{-i\boldsymbol{k}\cdot\boldsymbol{\alpha}_1} + t'e^{i\boldsymbol{k}\cdot\boldsymbol{\alpha}_2} + te^{-i\boldsymbol{k}\cdot\boldsymbol{\alpha}_2} + t'e^{i\boldsymbol{k}\cdot(\boldsymbol{\alpha}_1-\boldsymbol{\alpha}_2)} + te^{i\boldsymbol{k}\cdot(\boldsymbol{\alpha}_2-\boldsymbol{\alpha}_1)}]\} - 1 = 0. \tag{B21}$$

Using the parametrization of the S matrix given in Eq. (1) and the hexagonal lattice vectors $\boldsymbol{\alpha_1} = \frac{3}{2}\boldsymbol{x} + \frac{\sqrt{3}}{2}\boldsymbol{y}$, $\boldsymbol{\alpha_2} = \frac{3}{2}\boldsymbol{x} - \frac{\sqrt{3}}{2}\boldsymbol{y}$, we obtain the band structure $\phi(k_x,k_y)$ as

$$\begin{aligned} &e^{i6\phi}e^{i3\varphi} + e^{i3\phi}\cos^3\theta\left\{e^{i3\xi} - e^{i3(\varphi-\xi)} + \tan^2\theta e^{i\varphi}\left[2\cos\left(\frac{3k_x}{2}\right)(e^{i\xi}e^{i(\sqrt{3}/2)k_y} - e^{i(\varphi-\xi)}e^{-i(\sqrt{3}/2)k_y})\right.\right. \\ &\left.\left. - e^{i(\varphi-\xi)}e^{i\sqrt{3}k_y} + e^{i\xi}e^{-i\sqrt{3}k_y}\right]\right\} - 1 = 0. \end{aligned} \tag{B22}$$

Note that this expression does not depend on χ. Since Eq. (B22) is a quadratic polynomial in $e^{i3\phi}$, a band gap closing at some point (k_x^0,k_y^0) in the Brillouin zone corresponds to a vanishing value of its discriminant, i.e. (at least) two roots are degenerate. The locations of such band gap closings in the $(\theta,\xi,\varphi,\chi)$ parameter space of the system define boundaries between different insulator phases, which may have different topological order. Figure 2 shows a slice of the phase diagram of the honeycomb network model for $\varphi = \chi = 0$.

For $\varphi = 0$ (which corresponds to $\det[S] = 1$), we can simplify Eq. (B22) to

$$e^{i6\phi} + e^{i3\phi}\cos^3\theta\left\{2i\sin(3\xi) + \tan^2\theta\left[2\cos\left(\frac{3k_x}{2}\right)2i\sin\left(\frac{\sqrt{3}}{2}k_y + \xi\right) - 2i\sin(\sqrt{3}k_y - \xi)\right]\right\} - 1 = 0, \tag{B23}$$

and setting $\xi = \pi/2$ enables us to further simplify the band-structure equation to obtain

$$e^{i6\phi} + e^{i3\phi}\cos^3\theta\left\{-2i + \tan^2\theta\left[4i\cos\left(\frac{3}{2}k_x\right)\cos\left(\frac{\sqrt{3}}{2}k_y\right) + 2i\cos(\sqrt{3}k_y)\right]\right\} - 1 = 0. \tag{B24}$$

Defining $f(\boldsymbol{k})$ as

$$f(\boldsymbol{k}) \equiv 4\cos\left(\frac{3}{2}k_x\right)\cos\left(\frac{\sqrt{3}}{2}k_y\right) + 2\cos(\sqrt{3}k_y), \tag{B25}$$

we obtain

$$e^{i6\phi} + e^{i3\phi}\cos^3\theta\, i[-2 + \tan^2\theta f(\boldsymbol{k})] - 1 = 0. \tag{B26}$$

In the tight-binding regime ($\theta \approx 0$), this gives

$$e^{i3\phi_\pm} \approx \pm\theta\sqrt{3 + f(\boldsymbol{k})} + i, \tag{B27}$$

which yields

$$\phi_\pm \propto \pm\frac{\theta}{3}\sqrt{3 + f(\boldsymbol{k})}, \tag{B28}$$

in agreement with the standard result for the tight-binding Hamiltonian of graphene when only the nearest-neighbor coupling is taken into account [54]. The coefficient $\theta/3$ plays the role of the nearest-neighbor hopping energy.

[1] D. J. Thouless, M. Kohmoto, M. P. Nightingale, and M. den Nijs, Phys. Rev. Lett. **49**, 405 (1982).
[2] M. Stone, *Quantum Hall Effect* (World Scientific, Singapore, 1992).
[3] J. E. Moore, Nature (London) **464**, 194 (2010).
[4] M. Z. Hasan and C. L. Kane, Rev. Mod. Phys. **82**, 3045 (2010).
[5] X.-L. Qi and S.-C. Zhang, Rev. Mod. Phys. **83**, 1057 (2011).
[6] T. Oka and H. Aoki, Phys. Rev. B **79**, 081406 (2009).
[7] J. I. Inoue and A. Tanaka, Phys. Rev. Lett. **105**, 017401 (2010).
[8] T. Kitagawa, M. S. Rudner, E. Berg, and E. Demler, Phys. Rev. A **82**, 033429 (2010).
[9] T. Kitagawa, E. Berg, M. Rudner, and E. Demler, Phys. Rev. B **82**, 235114 (2010).
[10] N. H. Lindner, G. Refael, and V. Galitski, Nat. Phys. **7**, 490 (2011).
[11] Z. Gu, H. A. Fertig, D. P. Arovas, and A. Auerbach, Phys. Rev. Lett. **107**, 216601 (2011).
[12] J. Cayssol, B. Dóra, F. Simon, and R. Moessner, Phys. Status Solidi RRL **7**, 101 (2013).
[13] M. S. Rudner, N. H. Lindner, E. Berg, and M. Levin, Phys. Rev. X **3**, 031005 (2013).
[14] F. D. M. Haldane and S. Raghu, Phys. Rev. Lett. **100**, 013904 (2008).
[15] S. Raghu and F. D. M. Haldane, Phys. Rev. A **78**, 033834 (2008).
[16] Z. Wang, Y. D. Chong, J. D. Joannopoulos, and M. Soljačić, Phys. Rev. Lett. **100**, 013905 (2008).
[17] Z. Wang, Y. D. Chong, J. D. Joannopoulos, and M. Soljačić, Nature (London) **461**, 772 (2009).
[18] J. Koch, A. A. Houck, K. L. Hur, and S. M. Girvin, Phys. Rev. A **82**, 043811 (2010).
[19] A. Petrescu, A. A. Houck, and K. Le Hur, Phys. Rev. A **86**, 053804 (2012).
[20] A. B. Khanikaev, S. H. Mousavi, W.-K. Tse, M. Kargarian, A. H. MacDonald, and G. Shvets, Nat. Mater. **12**, 233 (2013).
[21] M. Hafezi, E. A. Demler, M. D. Lukin, and J. M. Taylor, Nat. Phys. **7**, 907 (2011).
[22] M. Hafezi, S. Mittal, J. Fan, A. Migdall, and J. M. Taylor, Nat. Photonics **7**, 1001 (2013).
[23] G. Q. Liang and Y. D. Chong, Phys. Rev. Lett. **110**, 203904 (2013).
[24] K. Fang, Z. Yu, and S. Fan, Nat. Photonics **6**, 782 (2012).
[25] M. C. Rechtsman, J. M. Zeuner, Y. Plotnik, Y. Lumer, D. Podolsky, F. Dreisow, S. Nolte, M. Segev, and A. Szameit, Nature (London) **496**, 196 (2013).
[26] F. D. M. Haldane, Phys. Rev. Lett. **61**, 2015 (1988).
[27] J. T. Chalker and P. D. Coddington, J. Phys. C **21**, 2665 (1988).
[28] D.-H. Lee, Z. Wang, and S. A. Kivelson, Phys. Rev. Lett. **70**, 4130 (1993).
[29] D.-H. Lee, Phys. Rev. B **50**, 10788 (1994).
[30] B. Kramer, T. Ohtsuki, and S. Kettemann, Phys. Rep. **417**, 211 (2005).
[31] R. Klesse and M. Metzler, Int. J. Mod. Phys. C **10**, 577 (1999).
[32] M. Janssen, M. Metzler, and M. R. Zirnbauer, Phys. Rev. B **59**, 15836 (1999).
[33] M. Janssen, *Fluctuations and Localization In Mesoscopic Electron Systems* (World Scientific, Singapore, 2001).
[34] R. B. Laughlin, Phys. Rev. B **23**, 5632 (1981).
[35] D. Meidan, T. Micklitz, and P. W. Brouwer, Phys. Rev. B **84**, 195410 (2011); see also I. C. Fulga, F. Hassler, and A. R. Akhmerov, *ibid*. **85**, 165409 (2012).
[36] C.-M. Ho and J. T. Chalker, Phys. Rev. B **54**, 8708 (1996).
[37] A. Yariv, IEEE Photonics Technol. Lett. **14**, 483 (2002).
[38] J. K. S. Poon, J. Scheuer, S. Mookherjea, G. T. Paloczi, Y. Huang, and A. Yariv, Opt. Express **12**, 90 (2004).
[39] R. Klesse and M. Metzler, Europhys. Lett. **32**, 229 (1995).
[40] A. P. Schnyder, S. Ryu, A. Furusaki, and A. W. W. Ludwig, Phys. Rev. B **78**, 195125 (2008).
[41] A. P. Schnyder, S. Ryu, A. Furusaki, and A. W. W. Ludwig, AIP Conf. Proc. **1134**, 10 2009).
[42] A. Kitaev, AIP Conf. Proc. **1134**, 22 (2009).
[43] T. Ozawa and I. Carusotto, arXiv:1307.6650.
[44] M. Hafezi, arXiv:1310.7946.
[45] C.-E. Bardyn, S. D. Huber, and O. Zilberberg, arXiv:1312.6894.
[46] J. T. Chalker and A. Dohmen, Phys. Rev. Lett. **75**, 4496 (1995).
[47] T. Kitagawa, M. A. Broome, A. Fedrizzi, M. S. Rudner, E. Berg, I. Kassal, A. Aspuru-Guzik, E. Demler, and A. G. White, Nat. Commun. **3**, 882 (2012).
[48] H. Obuse, A. Furusaki, S. Ryu, and C. Mudry, Phys. Rev. B **76**, 075301 (2007).
[49] H. Obuse, A. Furusaki, S. Ryu, and C. Mudry, Phys. Rev. B **78**, 115301 (2008).
[50] S. Ryu, C. Mudry, H. Obuse, and A. Furusaki, New J. Phys. **12**, 065005 (2010).
[51] T. Schwartz, G. Bartal, S. Fishman, and M. Segev, Nature (London) **446**, 52 (2007).
[52] M. Segev, Y. Silberberg, and D. N. Christodoulides, Nat. Photonics **7**, 197 (2013).
[53] F. Evers and A. D. Mirlin, Rev. Mod. Phys. **80**, 1355 (2008).
[54] A. Castro Neto, F. Guinea, N. M. R. Peres, K. S. Novoselov, and A. K. Geim, Rev. Mod. Phys. **81**, 109 (2009).